Scientific Journal of Impact Factor (SJIF): 5.71
e-ISSN (O): 2348-4470
p-ISSN (P): 2348-6406

International Journal of Advance Engineering and Research Development

Volume 5, Issue 02, February -2018

5G mmWave Transmissions

EECE542 Wireless Communications: Project #3, Fall 2017

Arth D Chandra

Dept. ELECTRICAL & COMPUTER ENGINEERING
State University of New York at Binghamton,
NY 13902, USA

Abstract— *The global bandwidth shortage facing wireless carriers has motivated the exploration of the underutilized millimeter wave (mm-wave) frequency spectrum for future broadband cellular communication networks. There is, however, little knowledge about cellular mm-wave propagation in densely populated indoor and outdoor environments. Millimeter-wave (mm W) frequencies between 30 and 300 GHz are a new frontier for cellular communication that offers the promise of orders of magnitude greater bandwidths combined with further gains via beamforming and spatial multiplexing from multielement antenna arrays This paper presents small-scale fading and Large-scale fading for millimeter-wave Transmission which is vital for the design and operation of future fifth generation cellular networks. The main reason of using mm Wave is Global bandwidth shortage due to which Wireless service providers (W.S.P) are facing many challenges. The solution to this problem is solved by mm Wave which provide Greater frequency allocation at millimeter wave which is needed for 5G cellular communication , Highly directional beam forming antennas as Frequency range is from 25GHz to 300GHz and wavelength between 10mm to 1mm. and Finest Quality Of Service(QOS). The back-bone networks for 5G will move from copper cables to optical fiber cable to millimeter wave wireless communication.*

Index Terms*— path loss model; 25 GHz; 300 GHz; 5G; millimeter wave; Cellular systems; channel models; millimeter wave radio; wireless propagation*

I. INTRODUCTION

To date, four generations of cellular communication systems have been adopted in the USA with each new mobile generation emerging every 10 years or so since around 1980: first generation analog FM cellular systems in 1981; second generation digital technology in 1992, 3G in 2001, and 4G LTE-A in 2011

Technology / Features	*1G*	*2/2.5G*	*3G*	*4G*	*5G*
Start/ Deployment	1970/ 1984	1980/ 1999	1990/ 2002	2000/ 2010	2010/ 2015
Data Bandwidth	2 kbps	14.4-64 kbps	2 Mbps	200 Mbps to 1 Gbps for low mobility	1 Gbps and higher
Standards	AMPS	2G: TDMA, CDMA, GSM 2.5G: GPRS, EDGE,1xRTT	WCDMA, CDMA-2000	Single unified standard	Single unified standard
Technology	Analog cellular technology	Digital cellular technology	Broad bandwidth CDMA, IP technology	Unified IP and seamless combination of broadband, LAN/WAN/	Unified IP and seamless combination of broadband,

First generation cellular networks were basic analog systems designed for voice communications. A move to early data services and improved spectral efficiency was realized in 2G systems through the use of digital modulations and time division or code division multiple access. 3G introduced high-speed Internet access, highly improved video and audio streaming capabilities by using technologies such as Wideband Code Division Multiple Access (W-CDMA) and High-Speed Packet Access (HSPA). HSPA is an amalgamation of two mobile telephony protocols, High Speed Downlink Packet Access (HSDPA) and High-Speed Uplink Packet Access (HSUPA), which extends and improves the performance of existing 3G mobile telecommunication networks utilizing WCDMA protocols. An improved 3GPP (3rd Generation Partnership Project) standard, Evolved HSPA (also known as HSPA+), was released in late 2008 with subsequent worldwide utilization beginning in 2010. HSPA has been deployed in over 150 countries by more than 350 communications service providers (CSP) on multiple frequency bands and is now the most extensively sold radio technology worldwide although LTE is closing the gap rapidly. The International Mobile Telecommunications-Advanced (IMT-Advanced) standard is the next-generation of mobile communications technology defined by the ITU and includes capabilities outstripping those of IMT-2000 (3G) mobile communication. ITU refers to IMT-Advanced as a 4G mobile communications technology, although it should be noted that there is no universally accepted definition of the term 4G.

LTE radio access technology has been developed by the 3GPP to offer a fully 4G-capable mobile broadband platform . LTE is an orthogonal frequency-division multiplexing (OFDM)-based radio access technology that supports a scalable transmission bandwidth up to 20 MHz and advanced multi-antenna transmission. As a key technology in supporting high data rates in 4G systems, Multiple-Input Multiple-Output (MIMO) enables multi-stream transmission for high spectrum effi- ciency, improved link quality, and adaptation of radiation patterns for signal gain and interference mitigation via adaptive beamforming using antenna arrays . The coalescence of HSPA and LTE will increase the peak mobile data rates of the two systems, with data rates exceeding 100 Mbps, and will also allow for optimal dynamic load balancing between the two technologies . As the demand for capacity in mobile broadband communications increases dramatically every year, wireless carriers must be prepared to support up to a thousand-fold increase in total mobile traffic by 2020, requiring researchers to seek greater capacity and to find new wireless spectrum beyond the 4G standard . To improve the existing LTE network, the wireless technology roadmap now extends to IMT-Advanced with LTE-Advanced defined to meet IMT-Advanced requirements, which will be theoretically capable of peak throughput rates that exceed 1 Gigabit per second (Gbps). LTE Advanced supports heterogeneous networks with co-existing large macro, micro, and pico cells, and Wi-Fi access points. Low cost deployment will be realized by self-organizing features and repeaters/relays

II. 5G MM WAVE INTRODUCTION

Wireless data traffic has been increasing at a rate of over 50% per year per subscriber, and this trend is expected to accelerate over the next decade with the continual use of video and the rise of the Internet-of-Things (IoT). To address this demand, the wireless industry is moving to its fifth generation (5G) of cellular technology that will use millimeter wave (mm Wave) frequencies to offer unprecedented spectrum and multi-Gigabit-per-second (Gbps) data rates to a mobile device. Mobile devices such as cell phones are typically referred to as user equipment (UE). A simple analysis illustrated that 1 GHz wide channels at 28 or 73 GHz could offer several Gbps of data rate to UE with modest phased array antennas at the mobile handset, and early work showed 15 Gbps peak rates are possible with 4 × 4 phased arrays antenna at the UE and 200 m spacing between base stations (BSs). Promising studies such as these led the US Federal Communications Commission (FCC) to authorize its 2016 “Spectrum Frontiers” allocation of 10.85 GHz of millimeter wave spectrum for 5G advancements, and several studies have proposed new mobile radio concepts to support 5G mobile networks.

5G mm Wave wireless channel bandwidths will be more than ten times greater than today’s 4G Long-Term Evolution (LTE) 20 MHz cellular channels. Since the wavelengths shrink by an order of magnitude at mm Wave when compared to today’s 4G microwave frequencies, diffraction and material penetration will incur greater attenuation, thus elevating the importance of line of-sight (LOS) propagation, reflection, and scattering. Accurate propagation models are vital for the design of new mm Wave signaling protocols (e.g., air interfaces). Over the past few years, measurements and models for a vast array of scenarios have been presented by many companies and research groups

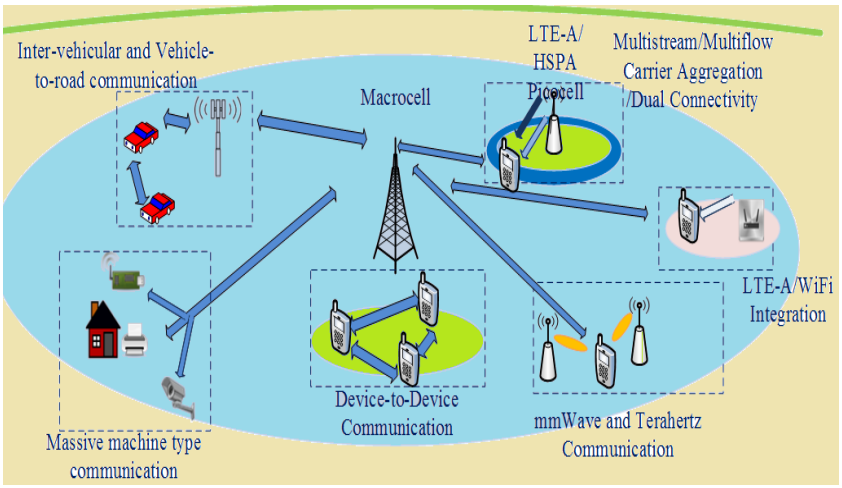

III. 5G SECURITY

As the 5G era is drawing near, the volume of data traffic and variety of services will increase to unseen-before levels. IoT service is just one of the many. When it comes to 5G, it is not simply about being a medium for communication. 5G security design is an all-encompassing one that provides security protection for the everything-connected world.

- E2E Security for Vertical Industries
- Secure Infrastructure
- Hybrid Authentication Management
- Diversified Identity Management
- Build E2E Security
- Isolate Virtual Network Slices

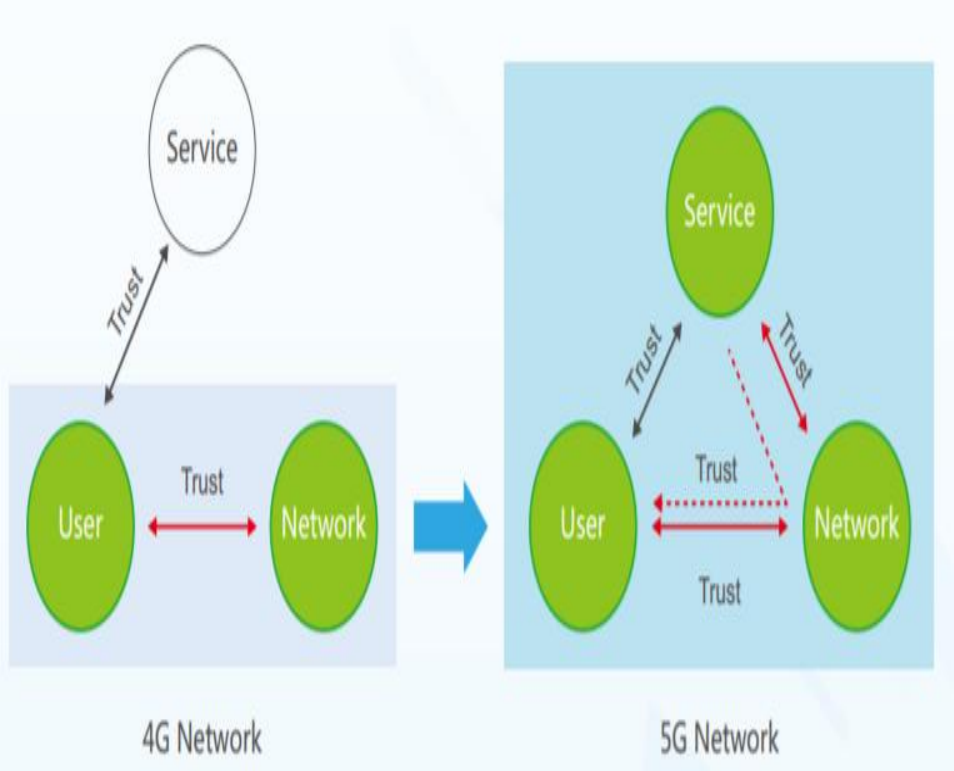

IV. 5G ANTENNA ARRAY

Narrow beam is the new feature of mm-wave. They reduce fading, multi-path losses, and interference ′ Antenna geometry is at chip size. The physical size of antennas is so small. This becomes practical to build complex antenna arrays. ′ Further integrate them on chip or PCB. This enables to create several arrays smart antenna which is adaptable in nature

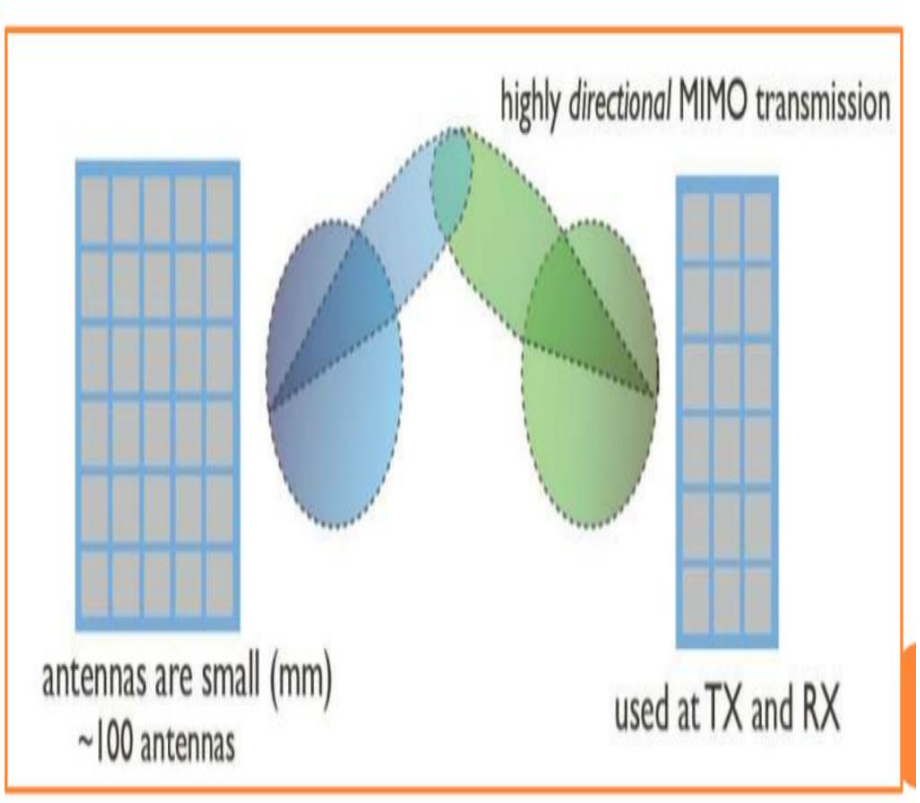

V. mm Wave Solution for 5G Communication System

Despite industrial research efforts to deploy the most efficient wireless technologies possible, the wireless industry always eventually faces overwhelming capacity demands for its currently deployed wireless technologies, brought on by the continued advances and discoveries in computing and communications, and the emergence of new customer handsets and use cases (such as the need to access the internet). This trend will occur in the coming years for 4G LTE, implying that at some point around 2020, wireless networks will face congestion, as well as the need to implement new technologies and architectures to properly serve the continuing demands of carriers and customers. The life cycle of every new generation of cellular technology is generally a decade or less (as shown earlier), due to the natural evolution of computer and communications technology. Our work contemplates a wireless future where mobile data rates expand to the multi gigabit-per-second range, made possible by the use of steerable antennas and mm-wave spectrum that could simultaneously support mobile communications and backhaul, with the possible convergence of cellular and Wi-Fi services. Recent studies suggest that mm-wave frequencies could be used to augment the currently saturated 700 MHz to 2.6 GHz radio spectrum bands for wireless communications . The combination of cost-effective CMOS technology that can now operate well into the mm-wave frequency bands, and high-gain, steerable antennas at the mobile and base station, strengthens the viability of mm-wave wireless communications ,Further, mm-wave carrier frequencies allow for larger bandwidth allocations, which translate directly to higher data transfer rates. Mm-wave spectrum would allow service providers to significantly expand the channel bandwidths far beyond the present 20 MHz channels used by 4G customers .By increasing the RF channel bandwidth for mobile radio channels, the data capacity is greatly increased, while the latency for digital traffic is greatly decreased, thus supporting much better internet-based access and applications that require minimal latency. Mm-wave frequencies, due to the much smaller wavelength, may exploit polarization and new spatial processing techniques, such as massive MIMO and adaptive beamforming . Given this significant jump in bandwidth and new capabilities offered by mm-waves, the base station-to-device links, as well as backhaul links between base stations, will be able to handle much greater capacity than today's 4G networks in highly populated areas. Also, as operators continue to reduce cell coverage areas to exploit spatial reuse, and implement new cooperative architectures such as cooperative MIMO, relays, and interference mitigation between base stations, the cost per base station will drop as they become more plentiful and more densely distributed in urban areas, making wireless back haul Equations

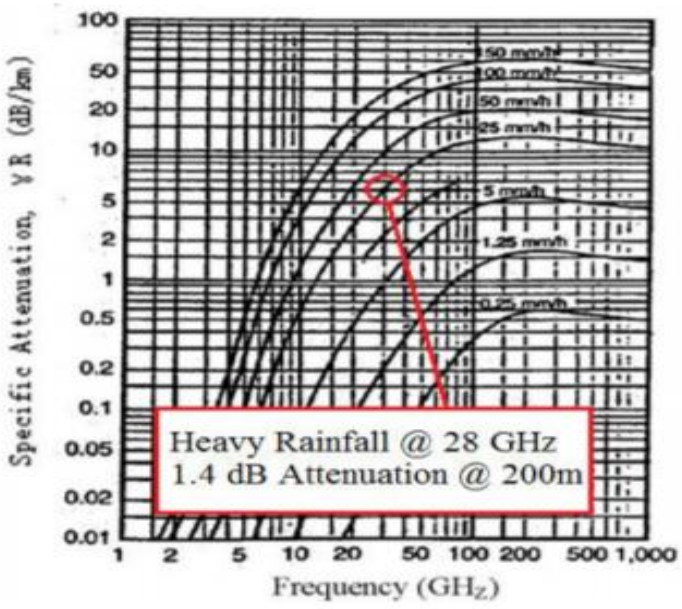

FIGURE 1. Rain attenuation in dB/km across frequency at various rainfall rates [26]. The rain attenuation at 28 GHz has an attenuation of 7 dB/km for a very heavy rainfall of 25 mm/hr (about 1 inch per hour). If cell coverage regions are 200 m in radius, the rain attenuation will reduce to 1.4 dB.

essential for flexibility, quick deployment, and reduced ongoing operating costs. Finally, as opposed to the disjointed spectrum employed by many cellular operators today, where the coverage distances of cell sites vary widely over three octaves of frequency between 700 MHz and 2.6 GHz, the mm-wave spectrum will have spectral allocations that are relatively much closer together, making the propagation characteristics of different mm-wave bands much more comparable and ''homogenous''. The 28 GHz and 38 GHz bands are currently available with spectrum allocations of over 1 GHz of bandwidth. Originally intended for Local Multipoint Distribution Service (LMDS) use in the late 1990's, these licensees could be used for mobile cellular as well as backhaul . A common myth in the wireless engineering community is that rain and atmosphere make mm-wave spectrum useless for mobile communications. However, when one considers the

fact that today's cell sizes in urban environments are on the order of 200 m, it becomes clear that mm-wave cellular can overcome these issues. Fig. 1 and Fig. 2 show the rain attenuation and atmospheric absorption characteristics of mm-wave propagation. It can be seen that for cell sizes on the order of 200 m, atmospheric absorption does not create significant additional path loss for mm-waves, particularly at 28 GHz and 38 GHz. Only 7 dB/km of attenuation is expected due to heavy rainfall rates of 1 inch/hr for cellular propagation at 28 GHz, which translates to only 1.4 dB of attenuation over 200 m distance. Work by many researchers has confirmed that for small distances (less than 1 km), rain attenuation will present a minimal effect on the propagation of mm-waves at 28 GHz to 38 GHz for small cells

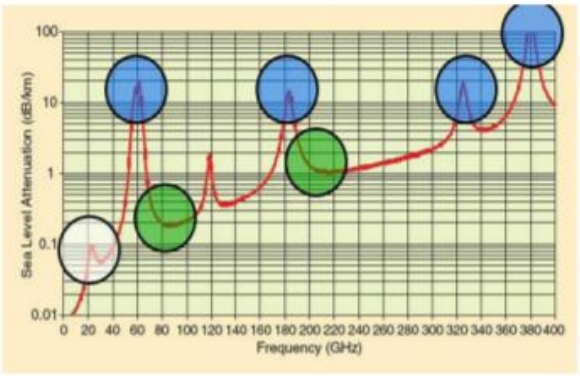

FIGURE 2. Atmospheric absorption across mm-wave frequencies in dB/km [1]. The attenuation caused by atmospheric absorption is 0.012 dB over 200 m at 28 GHz and 0.016 dB over 200 m at 38 GHz. Frequencies from 70 to 100 GHz and 125 to 160 GHz also have small loss.

VI.Understanding the Channel

Future wireless technologies must be validated in the most urban environments, such as New York City. In order to improve capacity and service quality, the cellular network architecture needs to support higher spatial reuse. Massive MIMO base stations and small-cell access points are two promising approaches for future cellular. Massive MIMO base stations allocate antenna arrays at existing macro base stations, which can accurately concentrate transmitted energy to the mobile users. Small cells offload traffic from base stations by overlaying a layer of small cell access points, which decreases the average distance between transmitters and users, resulting in lower propagation losses and higher data rates and energy efficiency .Both important trends are readily supported and, in fact, are enhanced by a move to mm-wave spectrum, since the tiny wavelengths allow for dozens to hundreds of antenna elements to be placed in an array on a relatively small physical platform at the base station, or access point, and the natural evolution to small cells ensures that mm-wave frequencies will overcome any attenuation due to rain. Understanding the radio channel is a fundamental requirement to develop future mm-wave mobile systems as well as backhaul techniques. With a firm technical understanding of the channel, researchers and industry practitioners may then explore new methods for the air interface, multiple access, architectural approaches that include cooperation and interference mitigation and other signal enhancement techniques. In order to create a statistical spatial channel model (SSCM) for mm-wave multipath channels, extensive measurements must be made in typical and worst-case operating conditions and environments. We have conducted extensive propagation measurements in urban environments in New York City and suburban environments in Austin, Texas in order to understand the mm-wave channel. Using the Template

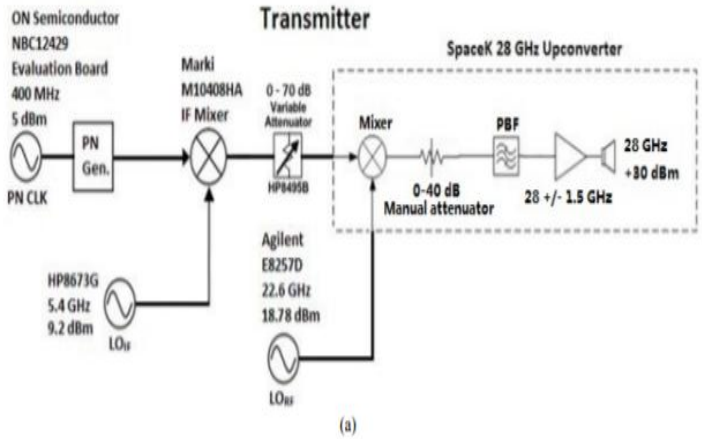

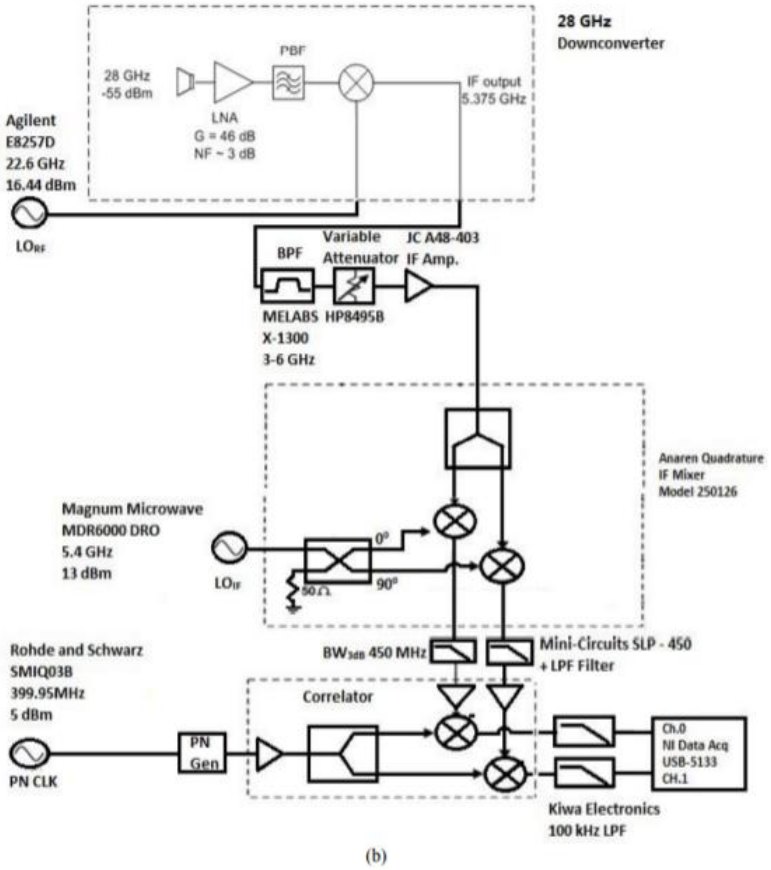

(b)

VII. Fading

In wireless communications, fading is variation or the attenuation of a signal with various variables. These variables include time, geographical position, and radio frequency. Fading is often modeled as a random process. A fading channel is a communication channel that experiences fading. In wireless systems, fading may either be due to multipath propagation, referred to as multipath induced fading, weather (particularly rain), or shadowing from obstacles affecting the wave propagation, sometimes referred to as shadow fading. Selection: Highlight all author and affiliation lines.

The presence of reflectors in the environment surrounding a transmitter and receiver create multiple paths that a transmitted signal can traverse. As a result, the receiver sees the superposition of multiple copies of the transmitted signal, each traversing a different path. Each signal copy will experience differences in attenuation, delay and phase shift while travelling from the source to the receiver. This can result in either constructive or destructive interference, amplifying or attenuating the signal power seen at the receiver. Strong destructive interference is frequently referred to as a deep fade and may result in temporary failure of communication due to a severe drop in the channel signal-to-noise ratio.

A. Large Scale Fading

Large-scale fading is the result of signal attenuation due to signal propagation over large distances and diffraction around large objects in the propagation path.

- **Relative Path Loss (loss due to distance)**

In free-space, the attenuation of a signal due to distance follows the $1/d^2$ law, where d is the distance between the transmitter and the receiver. This is the case for line-of-sight (LOS) signals (path B). In the case of non-line-of-sight (NLOS) signals (path A), the attenuation is more likely to be anywhere from $1/d^3$ to $1/d^6$. This additional loss of power in propagation channels occurs when part of the reflected signal is lost.

- **Shadowing**

Log normal shadowing is the result of the signal being blocked by large objects in the propagation path (path D). These are typically distant objects in the environment such as mountains, hills, or large buildings. The length of time it takes for a moving receiver to pass through the "shadow" of these obstacles brings about the term "slow fading". The statistical model used to describe shadowing is the log-normal distribution of the mean signal power.

B. Small Scale Fading

predict the variability of signal strength within short distances (several wavelengths)

- **Rayleigh Fading**

Rayleigh fading is used to simulate the rapid amplitude fluctuations where there is no direct ray component. Because there is no direct ray component, Rayleigh fading is often classified as the worst case fading type. Using a one ray model, this small-scale distribution simulates the effects of rapid amplitude fluctuations when the receiver travels a distance of a few wavelengths. The one ray is scattered near the receiver resulting arriving at the receiver from all directions (path C). The signals add in and out of phase giving rise to amplitude fluctuations that vary at a rate that is dependent on the speed of the receiver. The statistical model used to describe the amplitude variations is the Rayleigh probability distribution function. The receiver movement also produces a spreading of the signal in the frequency domain due to the Doppler effect. Signal's frequency changes when moving. Make the power loss time-varying

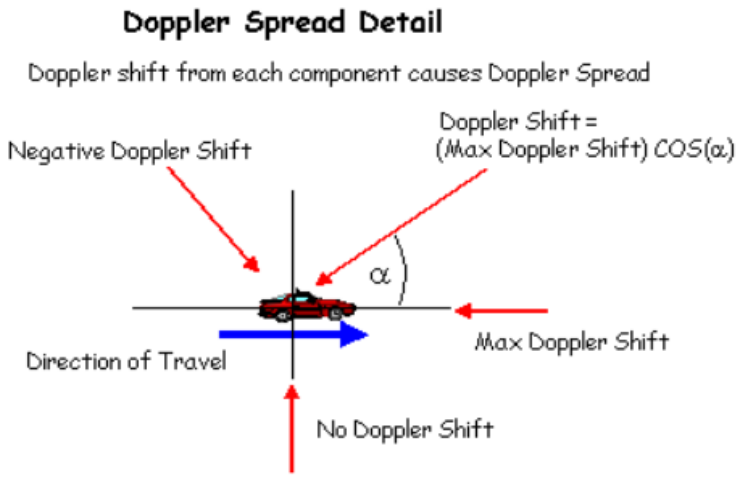

- **Multi Path Fading**

Multipath signals are received in a terrestrial environment, i.e., where different forms of propagation are present, and the signals arrive at the receiver from transmitter via a variety of paths. Therefore, there would be **multipath** interference, causing **multi- path fading**
Signals arrive along different paths, add destructively
Change significantly across very small distance.

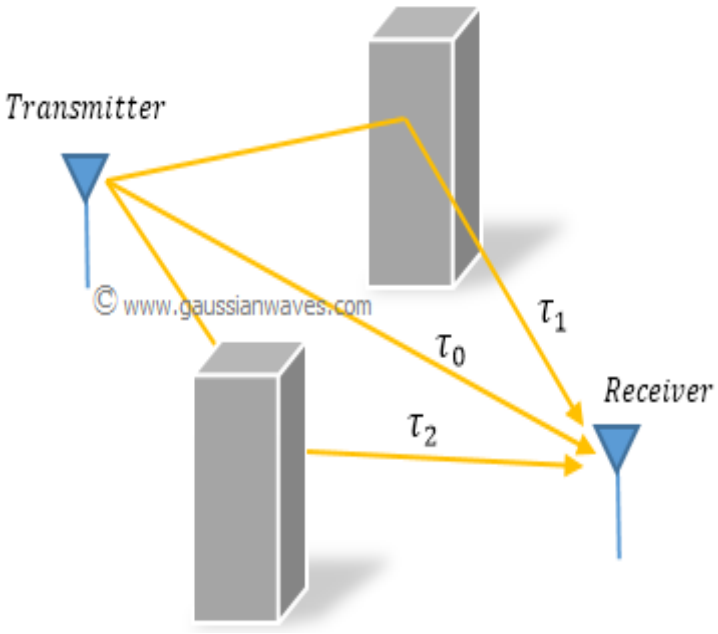

A. Large Scale PathLoss

Measurements for future outdoor cellular systems at 28 GHz and 38 GHz were conducted in urban microcellular environments in New York City. Measurements in both line-of-sight and non-line-of-sight scenarios used multiple combinations of steerable transmit and receive antennas Based on the measured data, we present path loss models suitable for the development of fifth generation (5G) standards. researchers have focused on abundant millimeter wave spectrum as a potential candidate for 5G cellular systems Measurements in New York CityTo provide a realistic assessment of mm W propagationin urban environments, our team conducted extensivemeasurements of 28- and 73-GHz channels in NYC.The 28- and 73-GHz bands were selected since they areboth likely to be initial frequencies where mm W cellularsystems could operate. The 28-GHz bands were previouslytargeted for LMDSs and are now attractive for initialdeployments of mm W cellular, given their relatively lowerfrequency within the mm W range. However, as mm Wsystems become more widely deployed, these lowerfrequency mm W bands will likely become depleted,particularly since they must compete with existing cellularbackhaul systems. Expansion to the higher bands is thusinevitable. In contrast, the E-band frequencies (71–76 GHzand 81–86 GHz) have abundant spectrum and areadaptable for dense deployment, providing a major optionfor carrier-class wireless indoor and outdoor transmission,should the lower frequency become congested. As shownin Fig. 1, the atmospheric absorption of E-band is onlyslightly worse (e.g., 1 dB/km) than today's widely usedlower frequency (UHF/microwave) bands.To measure the channel characteristics in thesefrequencies, we emulated microcellular-type deploymentswhere transmitters were placed on rooftops two to fivestories high and measurements were then made at anumber of street level locations up to 500 m from thetransmitters (see Fig. 5). To characterize both the bulkpath loss and the spatial structure of the channels,measurements were performed with highly directional, rotatable horn antennas [30-dBm RF output, 10 beam widths and 24.5-dBi gain at both transmitter (TX) and receiver b(RX)]. In order to obtain high time resolution, we employed a 400-Mcps (megachip per second) channel sounder (see Fig. 6). At each TX–RX location pair, the angles of the TX and RX antennas were swept across a range of values to
detect discrete clusters of paths

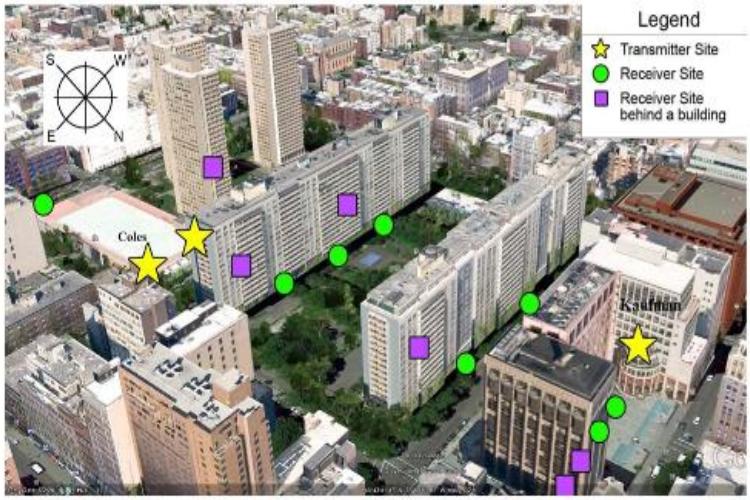

Fig. 5. *Image from [29] showing typical measurement locations in NYC at 28 GHz for which the isotropic path loss models in this paper are derived. Similar locations were used for the 73-GHz study.*

28 GHZ AND 38 GHZ PATH LOSS MODELS IN URBAN MICROCELLS

In the most general case, path loss, which is scaled in dB relative to a reference power or transmitted power, is assumed to have a linear dependence with logarithmic distance, expressed as:

$$\overline{PL(d)}(dB) = \alpha + \overline{\beta} \cdot 10\log_{10}(d) \qquad (1)$$

PL	Alpha	Beta	d
32.9894	2.2654	1.5362	100
143	5.365	6.325	150

where $\overline{\ }$ PL(d) is mean path loss over all distances in dB, α is the floating intercept in dB, β is linear slope (e.g. the average path loss exponent), and d is distance (TX-RX separation). In other, path loss can be derived as an extension to (1), including the dependence of frequency, shown as:

$$\overline{PL(d,f)}(dB) = \alpha + \beta \cdot 10\log_{10}(d) + \gamma \cdot 20\log_{10}\left(\frac{f}{f_c}\right) \quad (2)$$

PL	Alpha	Beta	d	Gamma	f	fc
-32.2	2.2654	1.5362	100	15 db	1Mhz	3*10^8
143	5.365	6.325	150	-15db	5Mhz	3*10^8

where γ is the frequency-dependency factor and f/fc is the ratio of the frequency deviation about the center carrier frequency. For the WINNER II model, the target frequency f ranged from 2-6 GHz with center frequency fc at 5 GHz For the measurements in New York City and Austin, only two carrier frequencies were employed, thus more data is needed to include frequency in path loss models for the mm-wave bands, and current work is being done by the authors at 72 GHz (Eband) for this purpose. Generally, the linear slope β is extracted by a best-fit linear regression to (1) or (2) using path loss values in dB scale, versus the logarithm of measurement distances. The path loss values are computed from the measured PDPs by integrating the area under the PDP to obtain received signal power at each location and antenna pointing angle, and then normalizing to the transmitted power and antenna gains to obtain channel path loss at each location and at each antenna pointing combination. The estimate approach employed is the least-square linear regression fit, in which the linear slope β can be derived by

$$\overline{\beta} = \frac{\sum_i^n \left(d_i - \overline{d}\right) \times \left(PL_i - \overline{PL}\right)}{\sum_i^n \left(d_i - \overline{d}\right)^2} \quad (3)$$

where di is the distance in dB scale of the i th measurement PDP for a given antenna pointing angle and RX location, d is the average distance in dB of all di in dB from the measurement snapshot, PLi is the path loss value of the i th measurement snapshot in dB and PL is the average path loss of the entire data set in dB, respectively. The constant α in dB is the floating intercept of the linear regression fit in (1) that fits the data empirically, and can be thought of as a globally optimum reference attenuation set point that determines the tilt of the path loss model (1), and is found as [15]:

$$\alpha(dB) = \overline{PL}(dB) - \overline{\beta} \cdot \overline{10\log_{10}(d)} \quad (4)$$

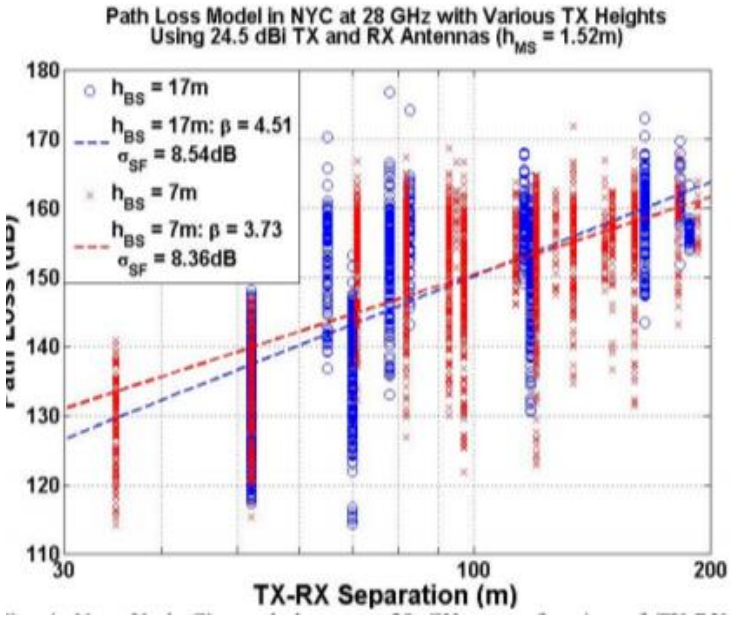

Fig. 4. New York City path losses at 28 GHz as a function of TX-RX separation distance at 28 GHz. The blue circles and red crosses are recorded path loss values extracted from PDPs. The dashed red and blue lines represent least-square fits through the path losses recorded in the measurement campaign for base station heights of 7m and 17m respectively. The slopes of the red and blue dashed lines are 3.73 and 4.51, while shadow fading factors are 8.36 dB and 8.54 dB, respectively

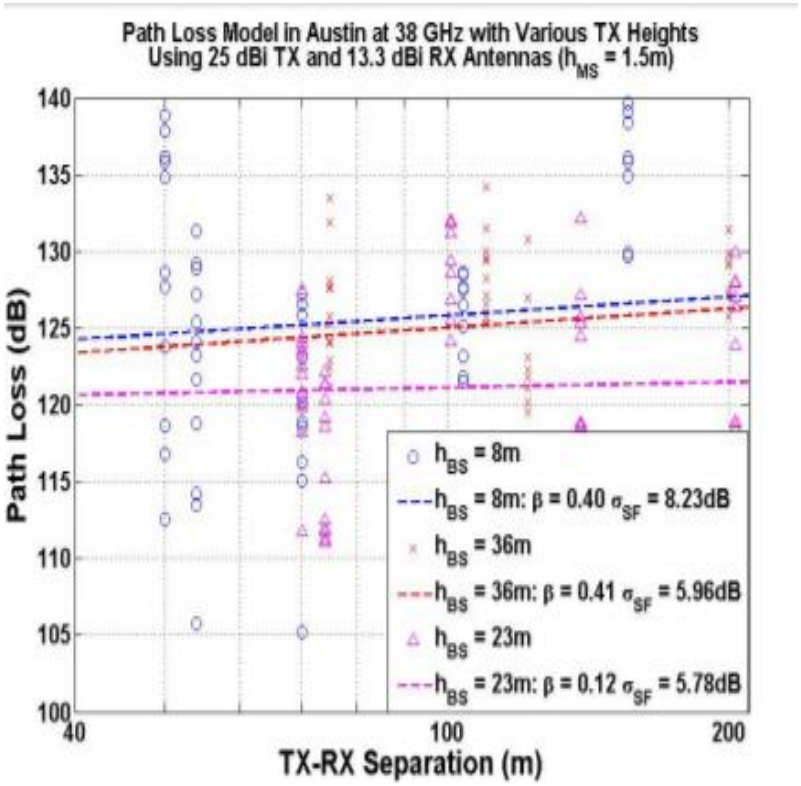

Fig. 5. Austin path losses at 38 GHz as a function of TX-RX separation distance at 38 GHz with 13.3 dBi RX antennas. The blue circles, purple triangles and red crosses are path loss values extracted from PDPs. The dashed blue, magenta and red lines represent least-square fits for base stations heights of 8m, 23m, and 36m respectively from the Austin measurement campaign. The slopes of the blue, magenta and red dashed lines are 0.40, 0.12 and 0.41 while shadow fading factors are 8.23 dB, 5.78 dB and 5.96 dB, respectively

Frequency	Tx height	Rx height	Path loss	Tx, Rx antenna gain	Tx,Rx separate	A	B	s
28Ghz (NY)	7	15	NOS	24.5	30<d <200	3.7	75	8
28Ghz (NY)	17	15	NOS	24.5	30<d <200	4.5	59	8
38Ghz	8	15	NOS	25	30<d <200	1.2	115	7
38Ghz	8	15	NOS	25,133	30<d <200	0.4	118	8
38Ghz	23	15	NOS	25,133	30<d <200	0.4	127	5
38Ghz	36	15	NOS	25,25	30<d <200	0.1	116	6

SMALL-SCALE FADING

The 28 GHz street-canyon small-scale fading measurements were performed on the NYU Brooklyn campus, using a 400 megachips-per-second broadband sliding correlator channel sounder, whose superheterodyne architecture is outlined in . The transmitter (TX) and receiver (RX) each used 15 dBi (28.8◦ and 30◦ half-power beamwidths in azimuth and elevation, respectively) directional horn antennas, with distances from the TX antenna to center of the RX local area ranging from 8 m to 12.9 m, with maximum TX power of 27 dBm. The largest measurable path loss was approximately 157 dB, with a 2.5 ns multipath time resolution (800 MHz RF null-tonull bandwidth). Directional antennas were utilized to emulate future mmWave systems that will consider electrically-steered multi-element antenna arrays and beamforming algorithms to enable high antenna gains at the TX and RX. The models presented

herein are valid after beam searching is performed while the mobile device is in motion. The ultrawideband measurements investigated spatial and temporal fading and autocorrelations of the received multipath signal amplitudes over a local area for vertical-to-vertical (V-V) and vertical-to-horizontal (V-H) antenna polarization scenarios. One TX location, Bridge (BRI), and four RX locations were selected to conduct the measurements in LOS, NLOS, and a transitional LOS-to-NLOS environment to gain insight into the statistics of multipath component amplitudes in realistic mobile environments, as depicted in Fig. 1. At each location, the RX antenna was moved over a stationary 35.31- cm spatial linear track (33 wavelengths) in steps of $\lambda/2 = 5.35$ mm, and for each track position a power delay profile (PDP) measurement was acquired. Each PDP capture was an average of 20 consecutive PDPs, with a total PDP capture time of 818.8 ms. The TX and RX antennas remained fixed in azimuth and elevation during the measurement captures, and were positioned 4 m and 1.4 m above ground level, respectively, well below surrounding rooftop heights of approximately 40 m. In total, 66 PDPs were acquired over one track length measurement. The linear track was positioned such that the RX antenna could be spatially incremented towards the TX antenna, and laterally from left to right of the static TX beam, so as to capture the channel fading over two orthogonal receiver directions, as illustrated with arrows in Fig. 1. The spatial track laid entirely within the 3-dB beamwidth of the TX antenna for the two LOS locations to minimize the effects of antenna beamwidth, thus removing the need to de-embed the antenna patterns from the measurements. Fig. 2 shows a photo of the linear track used during the measurements.

III. CHANNEL IMPULSE RESPONSE MODEL

The propagation channel is commonly described by the superposition of multiple traveling waves, where each impingFig. 1: Map of NYU Brooklyn campus, where the 28 GHz smallscale fading outdoor measurements were conducted in a street canyon scenario, with one TX location (BRI), and four RX locations. The black arrows originating from the TX show the azimuth AODs used for each RX local area, while the orthogonal arrows represent the two axes of a cross over which a power measurement was made every 5.35 mm to simulate a virtual array of directional antennas. Fig. 2: The small-scale linear track used to study small-scale signal fading over fractions of wavelengths. ing wave at the receiver is described by a complex (voltage) path amplitude, a delay, an azimuth and elevation AOD, and an azimuth and elevation AOA. The double-directional timeinvariant complex baseband channel impulse response (CIR) homni(t, −→Θ, −→Φ)

$$h_{omni}(t, \vec{\Theta}, \vec{\Phi}) = \sum_{k=1}^{N} a_k e^{j\theta_k} \delta(t - \tau_k) \cdot \delta(\vec{\Theta} - \vec{\Theta_k}) \cdot \delta(\vec{\Phi} - \vec{\Phi_k}) \quad (1)$$

where ak, θk, and τk are the amplitude, phase, and propagation delay of the k th multipath component, −→Θk = (θTX, φTX) and −→Φk = (θRX , φRX) are the vectors of azimuth and elevation AOD and AOA of the k th multipath component; N is the total number of resolvable multipath components, and δ() is the Dirac delta function. Thus, each multipath tap in the tap delay line model shown in (1) has seven associated multipath parameters. Measurement-based statistical distributions for |ak| 2 , τk, −→Θk and −→Φk in (1) have been extracted from 28 GHz ultrawideband propagation measurements using the time cluster - spatial lobe (TCSL) clustering approach [8], and the phases θk can be assumed independently and identically distributed uniformly between 0 and 2π. While (1) applies for an omnidirectional transmitter and receiver, it must be modified to reflect directional beam positioning during a real-time mmWave base-to-mobile communication link, similar to the measurements presented here. The directional CIR hdir(t), with fixed TX and RX antenna beam pointing directions, and for arbitrary TX and RX antenna patterns, can be expressed as

$$h_{dir}(t, \vec{\Theta_0}, \vec{\Phi_0}) = \sum_{k=1}^{M} a_k e^{j\theta_k} \delta(t - \tau_k) \cdot g_{TX}(\vec{\Theta_0} - \vec{\Theta_k}) \cdot g_{RX}(\vec{\Phi_0} - \vec{\Phi_k}) \quad (2)$$

where (−→Θ0, −→Φ0) are the fixed TX and RX beam pointing angles during the measurements, M is the total number of resolvable multipath components for the (−→Θ0, −→Φ0) pointing direction (corresponding to a subset of the total number N multipath components for omnidirectional transmissions and receptions from (1) , and gTX(−→Θ) and gRX(−→Φ) are the 3-dimensional (3-D) (azimuth and elevation) TX and RX complex amplitude antenna patterns of arbitrary multielement antenna arrays. Here, using directional horn antennas, 10 · log10(|gTX(0, 0)| 2) = 10 · log10(|gRX(0, 0)| 2) = 15 dBi. The statistics of the path gain amplitudes ak are studied for sub-wavelength receiver motion in a realistic future mmWave scenario, where the base station and mobile terminal are capable of beamforming in very narrow azimuth and elevation pointing directions, as shown in (2).

Analysis of Small-Scale Fading of Path Amplitudes

Small-scale spatial fading describes the random fluctuations of amplitudes of individual multipath components, as a mobile travels over a few wavelengths and experiences constructive interference from signals arriving within the measurement system resolution The small-scale spatial fading distributions were obtained for all individual multipath components over the local area, by discretizing the excess delay axis into bins, equal in time width to the transmitted pulse resolution, e.g., 2.5 ns. For a given delay bin, the individual multipath powers {|ak| 2} k=66 k=1 , whose powers were greater than the noise floor, were normalized by the mean (over the spatial dimension) bin power |ak| 2 (in the linear scale). Under the assumption that small-scale fading is delay independent the small-scale fading values of all resolvable paths at all delays were grouped into one dataset. Amplitude distributions about the local mean were extracted over the two orthogonal measured directions for the NLOS location (SS 4), the LOS-to-NLOS location (SS 3), and from the two LOS measured locations (SS 1 and SS 2). These were compared to a Rayleigh, Rician, and lognormal distribution. The Rayleigh distribution characterizes a scenario where many arriving multipath components have comparable delays and amplitudes, and its probability density function (PDF) is given by [26],

$$p_X(x) = \frac{x}{\sigma_n^2} e^{-x^2/2\sigma_n^2}$$

Px	x	Sigma
62.5	10	0.4
80	20	0.5
333	30	0.3

where σn is the standard deviation of the scattered multipath amplitudes. A Rician distribution indicates the presence of a specular dominant component in the channel over other very weak paths, and its PDF is expressed as

$$p_X(x) = \frac{x}{\sigma_n^2} e^{-\frac{x^2+A^2}{2\sigma_n^2}} I_0\left(\frac{Ax}{\sigma_n^2}\right)$$

$$K = \frac{A^2}{2\sigma_n^2}$$

where I0() is the modified Bessel function of the first kind and zero order, A is the amplitude of the dominant path, and σn is the standard deviation of all other weak path amplitudes. The PDF of a lognormal distribution is given by (6),

$$p_X(x) = \frac{1}{\sqrt{2\pi}\sigma x} e^{-(\log x - \overline{x})^2/2\sigma^2}$$

where x and σ are the mean and standard deviation, respectively

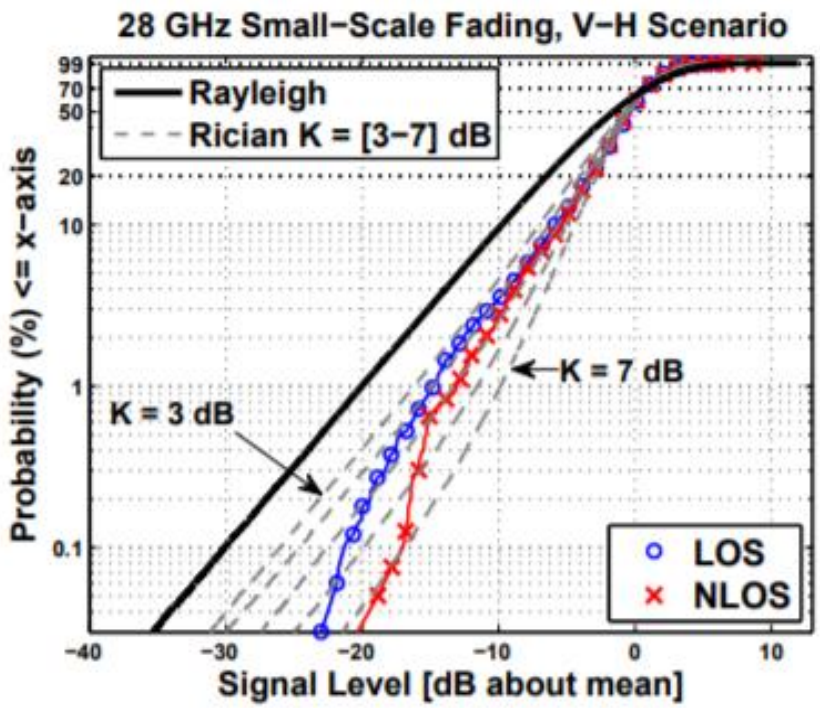

Transmission Power, Distance & Channel Capacity

a high data rate can be achieved by a combination of signal bandwidth and dynamic range. The limit for the data rate over a singleinput and single-output (SISO) link is set by the capacity (C) of the link and is a function of the bandwidth (BW) and the signal-to-noise ratio (SNR)

$$C = \mathrm{BW} \times \log_2(1 + \mathrm{SNR})$$

Capacity (C)	Bandwidth(BW)	SNR
152.6 Kbps	30KHz	15dB
2.0571Kbps	50KHz	-15dB

Therefore, a high data rate can be achieved with a low bandwidth if the SNR is high. However, a high SNR requires either a short distance between transmitter and receiver, or a high transmit power, or high gain antennas. This is described in the Friss Transmission equation:

$$P_{\mathrm{sig}} = P_t \times G_r \times G_t \times \left(\frac{\lambda}{4\pi \times d}\right)^{\alpha}$$

P sig	Pt	Gr	Gt	Lamda	Distance(d)	a
0.131W	50W	1	1	0.33	10	1
4.74uW	30W	1	1	0.5	100	2

d integrated noise power of the receiver can be expressed as

$$N_{\mathrm{in}} = k \times T \times \mathrm{NF} \times \mathrm{BW}$$

Nin	k	T	NF	BW
8*10^-15	1.38*10^(-23)	290	2dB	1MHz
6.21*10^-14	1.38*10^(-23)	300	3dB	5MHZ

Capacity With Noise

$$C = \mathrm{BW} \times \log_2\left(1 + \frac{P_t \times G_r \times G_t (\frac{\lambda}{4\pi \times d})^{\alpha}}{k \times T \times \mathrm{BW} \times \mathrm{NF}}\right)$$

C	BW	Psig	Nin
430.984MHz	10MHz	0.131W	8*10^-15
523.7MHz	20MHz	4.74uW	6.21*10^-14

Modulation

At present 4G LTE uses QAM with OFDM as modulation and OFDMA as access scheme. The challenge in 5G is high bit rate with mobility. Therefore, spectral efficiency is utmost important. The following indicate modulation schemes, which may find use in 5G implementations.

1. QAM with OFDM is a still contender.

2. Filter-bank multi-carrier (FBMC/OQAM) modulation. It exhibits better spectrum shape compared to the OFDM (Orthogonal Frequency-Division Multiplexing) and enables better spectrum usage and mobility support.

3. Single-carrier modulations (SCMs): This is still active and contender for 5G. The requirement is optimal equalization. The optimal equalization of a single carrier system is much more involved and essentially requires the use of a Viterbi algorithm.

4. Faster-than-Nyquist (FTN)/Time-frequency-packed (TFS) signaling: FTN multi-carrier is named as TFS. The TFS system has most of the parameters identical to FBMC. The TFS is implemented either with QAM or OQAM.

5. Wave modulation (WAM): WAM patented by MagnaComa is pure digital technique; a set of algorithms that implement a form of spectral compression. It fits into the signal processing path after the FEC, but before the digital front-end of the radio. WAM gives an overall 10% system gain advantage, up to 400% increase in range, a 50% spectrum savings, improved noise tolerance, and increase in data speed. One key benefit is the ability of the system to work with non-linear (such as class C) power amplifiers (PAs). It can be implemented in a DSP, but is more efficient in an FPGA or ASIC.

6. Cohere Technologies patented new modulation technology called Orthogonal Time Frequency and Space (OTFS), to increase the capacity.

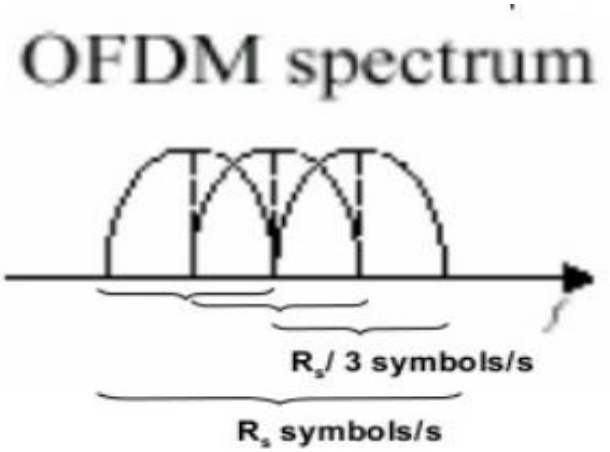

Challenges

Despite the potential of mmW cellular systems, there are a number of key challenges to realizing the vision of cellular networks in these bands. • Range and directional communication: Friis' transmission law [54] states that the free space omnidirectional path loss grows with the square of the frequency. However, the smaller wavelength of mmW signals also enables proportionally greater antenna gain for the same physical antenna size. Consequently, the

higher frequencies of mmW signals do not in themselves result in any increased free space propagation loss, provided the antenna area remains fixed and suitable directional transmissions are used. We will confirm this property from our measurements below; see, also,. However, the reliance on highly directional transmissions will necessitate certain design

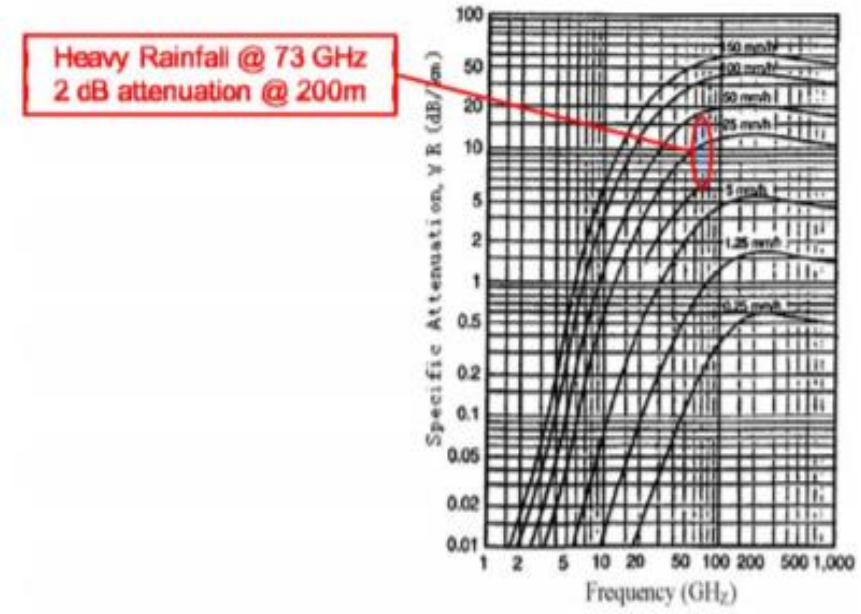

Fig. 2. ***Rain fades: Even in very heavy rainfall, rain fades are typically less than 1 dB per 100 m, meaning they will have minimal impact in cellular systems with cell radii less than 200 m. Figure from [32].***

changes to current cellular systems that we discuss in Section V. • Shadowing: A more significant concern for range is that mmW signals are extremely susceptible to shadowing. For example, materials such as brick can attenuate signals by as much as 40–80 dB and the human body itself can result in a 20–35-dB loss On the other hand, humidity and rain fadesVcommon problems for long-range mmW backhaul linksVare not an issue in cellular systems; see Fig. 2 and Also, the human body and many outdoor materials being very reflective allow them to be important scatterers for mmW propagation . • Rapid channel fluctuations and intermittent connectivity: For a given mobile velocity, channel coherence time is linear in the carrier frequency , meaning that it will be very small in the mmW range. For example, the Doppler spread at 60 km/h at 60 GHz is over 3 kHz, hence the channel will change in the order of hundreds of microseconds, much faster than today's cellular systems. In addition, high levels of shadowing imply that the appearance of obstacles will lead to much more dramatic swings in path loss, although beamsteering may overcome this Also, mmW systems will be inherently built of small cells, meaning that relative path losses and cell association also change rapidly. From a systems perspective, this implies that connectivity will be highly intermittent and communication will need to be rapidly adaptable. • Multiuser coordination: Current applications for mmW transmissions are generally for point-topoint links (such as cellular backhaul), or LAN and PAN systems with a limited number of users or MAC-layer protocols that prohibit multiple simultaneous transmissions. However, for high spatial reuse and spectral efficiency, cellular systems require simultaneous transmissions on multiple interfering links, and new mechanisms will be needed to coordinate these transmissions in mmW networks. • Processing power consumption: A significant challenge in leveraging the gains of multiantenna, wide-bandwidth mmW systems is the power consumption in the analog-to-digital (A/D) conversion. Power consumption generally scales linearly in the sampling rate and exponentially in the number of bits per samples making high-resolution quantization at wide bandwidths and large numbers of antennas prohibitive for low-power, low-cost devices. For example, scaling power consumption levels of even a state-of-the-art CMOS A/D converter designs such as and suggests that A/D converters at rates of 100 Ms/s at 12 b and 16 antennas would require more than 250 mW, a significant drain for current mobile devices. Also, efficient RF power amplification and combining will be needed for phased array antennas.

University of Bristol Researchers set up this 128-antenna array in March at the University of Bristol to carry out the first of several attempts to achieve greater spectrum efficiency.

Solution to the problem

A team of 5G researchers has done work for for spectrum efficiency. Their achievement with massive MIMO (multiple-input, multiple-output) arrays, which are cellular base stations comprised of dozens of antennas, is further evidence that this technology is a promising option for wireless engineers working to construct networks to deliver ultra-fast data speeds to more smartphones and tablets than ever before.

In an experiment, the group achieved a rate of 145.6 (bits/s)/Hz for 22 users, each modulated with 256-QAM, on a shared 20 MHz radio channel at 3.51 GHz with an 128-antenna massive MIMO array. That represents a 22-fold increase in spectrum efficiency over today's existing 4G networks.

The designed array would work best as part of ultra-dense small cell networks in cities, the company is working on massive MIMO for a different purpose—as a way to beam wireless internet to rural areas from within cities exchange much more information over the almost instant data transfer offered by 5G. But with consumers already facing a dwindling supply of spectrum, 5G to find ways to use the available spectrum to exchange all this new data more efficiently without causing delaysgroups are focused on massive MIMO, which allows for the simultaneous transfer of many incoming and outgoing messages at once. While traditional cellular base stations might rely on four antennas, a massive MIMO array features dozens that rely on signal processing to find the best and fastest way to route messages 1000-fold increase in capacity in order for 5G to function as envisioned. Not all of that increase must come from massive MIMO, contribution from millimeter wave and beamforming is also the need.

V. CONCLUSION

GIVEN THE WORLDWIDE NEED FOR CELLULAR SPECTRUM, AND THE RELATIVELY LIMITED AMOUNT OF RESEARCH DONE ON MM-WAVE MOBILE COMMUNICATIONS, WE HAVE PRESENTED SOME INITIAL PROPAGATION MEASUREMENTS IN NY WHICH ARE USED FOR OUTDOOR SMALL-SCALE & LARGE SCALE FADING MEASUREMENTS.USING WHICH WE DEFINE A MODEL FOR FADING .USING THE DATA WE ALSO FIND KEY FEATURE OF FADING MODEL LIKE TRANSMISSION POWER , TRANSMISSION DISTANCE & CHANCEL CAPACITY.

Considering the modulation to be used At present 4G LTE uses QAM with OFDM as modulation and OFDMA as access scheme but this scheme cannot be used in 5G as main aim is to reduce the overhead at the physical layer physical(PHY)overhead,New modulation and coding schemes (MCSs) to increase the spectrum efficiency such as in small-cell deployment scenarios having more favorable signal-to noise ratio (SNR) conditions than typical macrocell deployments. Well 5G is still an open issue. nothing is standardized. Some of the Strong Contenders for Modulation technical used are hybrid schemes like

- F-QAM or FSK-QAM.
- Filter-bank multi-carrier (FBMC/OQAM) modulation. It exhibits better spectrum shape compared to the OFDM & also provides better spectrum usage and mobility support.
- Single-carrier modulations (SCMs): This is still active and contender for 5G. The requirement is optimal equalization.
- Orthogonal Time Frequency and Space (OTFS), to increase the capacity.This paper has provided a comprehensive overview of emerging 5G mmWave wireless system concepts, and has provided a compilation of important mmWave radio propagation models developed throughout the world to date. The paper demonstrates early standards work and illustrates the various models obtained by several independent groups based on extensive measurements and ray tracing methods at mmWave frequency bands in various scenarios. The development of proper propagation models is vital, not only for the long-term development of future mmWave wireless systems but also for fundamental understanding by future engineers and students who will learn about and improve the nascent mmWave mobile industry that is just now being developed. Various companies have started 5G field trials, and some of them have achieved 20 Gbps date rates . The fundamental information on path loss and shadowing surveyed in this paper is a prerequisite for moving further along the road to 5G at the unprecedented mmWave frequency bands

ACKNOWLEDGMENT

THE AUTHORS WOULD LIKE TO THANK DR. XIAOHUA(EDWARD) LI, ASSOCIATE PROFESSOR OF ELECTRICAL ENGINEERING STATE UNIVERSITY OF NEW YORK AT BINGHAMTON THAT MADE THIS RESEARCH POSSIBLE.HIS KNOWLEDGE AND CONSTANT HELP MADE IT POSSIBLE FOR US TO UNDERSTAND THE CONCEPTS AND MAKE THIS REPORT POSSIBLE . THIS WORK ALSO BENEFITTED SIGNIFICANTLY" *PROCEEDINGS OF THE IEEE*, VOL. 102, NO. 3, PP. 366–385, MAR. 2014. S. RANGAN, T. RAPPAPORT, AND E. ERKIP, "MILLIMETER-WAVE CELLULAR WIRELESS NETWORKS: POTENTIALS AND CHALLENGES," *PROCEEDINGS OF THE IEEE*, VOL. 102, NO. 3, PP. 366–385, MAR. 2014.

REFERENCES

[1] T. S. Rappaport, R. W. Heath, Jr., R. C. Daniels, and J. N. Murdock, Millimeter Wave Wireless Communications. Pearson/Prentice Hall 2015.

[2] F. Khan and Z. Pi, "mmwave mobile broadband (MMB): Unleashing the 3 -300 GHz spectrum," in 2011 34th IEEE Sarnoff Symposium, May 2011, pp. 1–6.

[3] T. S. Rappaport et al., "Millimeter wave mobile communications for 5G cellular: It will work!" IEEE Access, vol. 1, pp. 335–349, 2013

[4] ——, "Wideband Millimeter-Wave Propagation Measurements and Channel Models for Future Wireless Communication System Design (Invited Paper)," IEEE Transactions on Communications, vol. 63, no. 9, pp. 3029–3056, Sept. 2015.

[5] K. Haneda, J. Jarvelainen, A. Karttunen, M. Kyro, and J. Putkonen, "Indoor short-range radio propagation measurements at 60 and 70 GHz," in 2014 8th European Conference on Antennas and Propagation (EuCAP), April 2014, pp. 634–638.

[6] S. Hur et al., "Proposal on Millimeter-Wave Channel Modeling for 5G Cellular System," IEEE Journal of Selected Topics in Signal Processing (JSTSP), 2015.

[7] M. K. Samimi and T. S. Rappaport, "3-D Statistical channel models for Millimeter-wave outdoor mobile broadband communications," in 2015 IEEE International Conference on Communications (ICC), June 2015, pp. 2430–2436.

[8] "Statistical Channel Model with Multi-Frequency and Arbitrary Antenna Beamwidth for Millimeter-Wave Outdoor Communications," in 2015 IEEE Global Telecommunications Conference (GLOBECOM), Workshop, Dec. 2015.

[9] "Ultra-Wideband Statistical Channel Model for 28 GHz Millimeter-Wave Urban NLOS Environments," in 2014 IEEE Global Telecommunications Conference (GLOBECOM 2014), Dec. 2014, pp. 3483–3489.

[10] S. Sun et al., "MIMO for Millimeter Wave Wireless Communications: Beamforming, Spatial Multiplexing, or Both?" IEEE Communications Magazine, vol. 52, no. 12, pp. 110–121, Dec. 2014.

[11] R. C. Bultitude, "Measurement, characterization and modeling of indoor 800/900 MHz radio channels for digital communications," IEEE Communications Magazine, vol. 25, no. 6, pp. 5–12, June 1987.

[12] T. S. Rappaport, S. Y. Seidel, and K. Takamizawa, "Statistical channel impulse response models for factory and open plan building radio communication system design," IEEE Transactions on Communications, vol. 39, no. 5, pp. 794–807, May 1991.

[13] H. Hashemi, D. Tholl, and T. Vlasschaert, "A study of CW spatial fading of the indoor radio propagation channel," in 1995 Fourth IEEE International Conference on Universal Personal Communications., Nov. 1995, pp. 201–205..

[14] P. Karttunen, K. Kalliola, T. Laakso, and P. Vainikainen, "Measurement analysis of spatial and temporal correlation in wideband radio channels with adaptive antenna array," in IEEE 1998 International Conference on Universal Personal Communications, vol. 1, Oct. 1998, pp. 671–675.

[15] "Spatial Channel Model for Multiple Input Multiple Output (MIMO) Simulations," Tech. Rep. 3GPP 25.996 V12.0.0, Sept. 2014.

[16] P. Kyosti et al., "WINNER II channel models," European Commission, IST-WINNER, Tech. Rep. D1.1.2, 2007, Sep 2007. [Online]. Available: http://projects.celticinitiative.org/winner+/WINNER2-Deliverables/

[17] G. Calcev, D. Chizhik, B. Goransson, S. Howard, H. Huang, A. Kogiantis, A. Molisch, A. Moustakas, D. Reed, and H. Xu, "A wideband spatial channel model for system-wide simulations," IEEE Transactions on Vehicular Technology, vol. 56, no. 2, pp. 389–403, March 2007.

[18] L. Liu, C. Oestges, J. Poutanen, K. Haneda, P. Vainikainen, F. Quitin, F. Tufvesson, and P. D. Doncker, "The COST 2100 MIMO channel model," IEEE Wireless Communications, vol. 19, no. 6, pp. 92–99, December 2012

[19] J. Kivinen, X. Zhao, and P. Vainikainen, "Empirical characterization of wideband indoor radio channel at 5.3 GHz," IEEE Transactions on Antennas and Propagation, vol. 49, no. 8, pp. 1192–1203, Aug. 2001.

[20] W. H. Tranter, K. S. Shanmugan, T. S. Rappaport, and K. L. Kosbar, Principles of Communication Systems Simulation with Wireless Applications. Prentice Hall Communications Engineering and Emerging Technologies Series 2004.

[21] V. Fung, T. S. Rappaport, and B. Thoma, "Bit error simulation for pi/4 DQPSK mobile radio communications using two-ray and measurementbased impulse response models," IEEE Journal on Selected Areas in Communications, vol. 11, no. 3, pp. 393–405, Apr. 1993.

[22] T. S. Rappaport and V. Fung, "Simulation of bit error performance of FSK, BPSK, and pi/4 DQPSK in flat fading indoor radio channels using a measurement-based channel model," IEEE Transactions on Vehicular Technology, vol. 40, no. 4, pp. 731–740, Nov. 1991.

[23] M. K. Samimi, S. Sun, and T. S. Rappaport, "MIMO Channel Modeling and Capacity Analysis for 5G Millimeter-Wave Wireless Systems," in the 10th European Conference on Antennas and Propagation (EuCAP'2016), April 2016.

[24] M. Steinbauer, A. Molisch, and E. Bonek, "The double-directional radio channel," IEEE Antennas and Propagation Magazine, vol. 43, no. 4, pp. 51–63, Aug. 2001.

[25]] S. Sun, G. R. MacCartney, M. K. Samimi, and T. S. Rappaport, "Synthesizing omnidirectional received power and path loss from directional measurements at millimeter-wave frequencies," 2015 IEEE Global Telecommunications Conference (GLOBECOM 2015), pp. 3948–3953, Dec. 2015.

[26] T. S. Rappaport, "Wireless Communications: Principles and Practice," in 2nd Edition, Prentice Hall Communications Engineering and Emerging Technologies Series, 2002.

[27] A. Saleh and R. Valenzuela, "A statistical model for indoor multipath propagation," IEEE Journal on Selected Areas in Communications, vol. 5, no. 2, pp. 128–137, February

.

